

**$\beta$ -delayed fission of isomers in  $^{188}\text{Bi}$** 

B. Andel<sup>1,2,\*</sup>, A. N. Andreyev<sup>3,4</sup>, S. Antalic<sup>2</sup>, M. Al Monthery<sup>3</sup>, A. Barzakh<sup>5</sup>, M. L. Bissell<sup>6</sup>, K. Chrysalidis<sup>7</sup>, T. E. Cocolios<sup>1</sup>, J. G. Cubiss<sup>3</sup>, T. Day Goodacre<sup>7,6,†</sup>, N. Dubray<sup>8</sup>, G. J. Farooq-Smith<sup>1</sup>, D. V. Fedorov<sup>5</sup>, V. N. Fedosseev<sup>7</sup>, L. P. Gaffney<sup>9,‡</sup>, R. F. Garcia Ruiz<sup>6,§</sup>, S. Goriely<sup>10</sup>, C. Granados<sup>1</sup>, R. D. Harding<sup>3,7</sup>, R. Heinke<sup>11</sup>, S. Hilaire<sup>8</sup>, M. Huyse<sup>1</sup>, J.-F. Lemaître<sup>10</sup>, K. M. Lynch<sup>7</sup>, B. A. Marsh<sup>7</sup>, P. Molkanov<sup>5</sup>, P. Mosat<sup>2</sup>, S. Péru<sup>8</sup>, C. Raison<sup>3</sup>, S. Rothe<sup>7</sup>, C. Seiffert<sup>7</sup>, M. D. Seliverstov<sup>5</sup>, S. Sels<sup>1,||</sup>, D. Studer<sup>11</sup>, J. Sundberg<sup>7,12</sup> and P. Van Duppen<sup>1</sup>

<sup>1</sup>*KU Leuven, Instituut voor Kern- en Stralingsfysica, B-3001 Leuven, Belgium*

<sup>2</sup>*Department of Nuclear Physics and Biophysics, Comenius University in Bratislava, 84248 Bratislava, Slovakia*

<sup>3</sup>*Department of Physics, University of York, York YO10 5DD, United Kingdom*

<sup>4</sup>*Advanced Science Research Center, Japan Atomic Energy Agency, Tokai-mura, Ibaraki 319-1195, Japan*

<sup>5</sup>*Petersburg Nuclear Physics Institute, NRC Kurchatov Institute, 188300 Gatchina, Russia*

<sup>6</sup>*School of Physics and Astronomy, The University of Manchester, Manchester M13 9PL, United Kingdom*

<sup>7</sup>*CERN, CH-1211 Geneva 23, Switzerland*

<sup>8</sup>*CEA, DAM, DIF, F-91297 Arpajon, France*

<sup>9</sup>*School of Engineering and Computing, University of the West of Scotland, Paisley, PA1 2BE, United Kingdom*

<sup>10</sup>*Institut d'Astronomie et d'Astrophysique, Université Libre de Bruxelles, CP 226, B-1050 Brussels, Belgium*

<sup>11</sup>*Institut für Physik, Johannes Gutenberg-Universität, Mainz, D-55128 Mainz, Germany*

<sup>12</sup>*Department of Physics, University of Gothenburg, SE-412 96 Gothenburg, Sweden*



(Received 13 February 2020; accepted 20 March 2020; published 24 July 2020)

$\beta$ -delayed fission ( $\beta$ DF) decay of a low-spin (ls) and a high-spin (hs) isomer in  $^{188}\text{Bi}$  was studied at the ISOLDE facility at CERN. Isomer-selective laser ionization and time gating were employed to investigate each isomer separately and their  $\beta$ DF partial half-lives were determined:  $T_{1/2p,\beta\text{DF}}(^{188}\text{Bi}^{\text{hs}}) = 5.6(8) \times 10^3$  s and  $T_{1/2p,\beta\text{DF}}(^{188}\text{Bi}^{\text{ls}}) = 1.7(6) \times 10^3$  s. This work is the first  $\beta$ DF study of two states in one isotope and allows the spin dependence of low-energy fission to be explored. The fission fragment mass distribution of a daughter nuclide  $^{188}\text{Pb}$ , following the  $\beta$  decay of the high-spin isomer, was deduced and indicates a mixture of symmetric and asymmetric fission modes. Experimental results were compared with self-consistent mean-field calculations based on the finite-range Gogny D1M interaction. To reproduce the measured  $T_{1/2p,\beta\text{DF}}(^{188}\text{Bi}^{\text{hs}})$ , the calculated fission barrier of  $^{188}\text{Pb}$  had to be reduced by  $\approx 30\%$ . After this reduction, the measured  $T_{1/2p,\beta\text{DF}}(^{188}\text{Bi}^{\text{ls}})$  was in agreement with calculations for a few possible configurations for  $^{188}\text{Bi}^{\text{ls}}$ . Theoretical  $\beta$ DF probabilities for these configurations were found to be lower by a factor of 4–9 than the  $\beta$ DF probability of  $^{188}\text{Bi}^{\text{hs}}$ . The fission fragment mass distribution of  $^{188}\text{Pb}$  was compared to the scission-point model SPY and the calculations based on the finite-range liquid-drop model. The first observation of  $\beta$ DF for  $^{190}\text{Bi}$  is also reported.

DOI: [10.1103/PhysRevC.102.014319](https://doi.org/10.1103/PhysRevC.102.014319)

**I. INTRODUCTION**

In the  $\beta$ -delayed fission ( $\beta$ DF) process [1,2], a parent nuclide first undergoes  $\beta$  decay to a state in the daughter nucleus

\*boris.andel@kuleuven.be

<sup>†</sup>Present address: TRIUMF, 4004 Wesbrook Mall, Vancouver, British Columbia, Canada V6T 2A3.

<sup>‡</sup>Present address: Oliver Lodge Laboratory, University of Liverpool, Liverpool L69 7ZE, United Kingdom.

<sup>§</sup>Present address: Department of Physics, Massachusetts Institute of Technology, Cambridge, MA 02139, USA.

<sup>||</sup>Present address: CERN, CH-1211 Geneva 23, Switzerland.

Published by the American Physical Society under the terms of the [Creative Commons Attribution 4.0 International](https://creativecommons.org/licenses/by/4.0/) license. Further distribution of this work must maintain attribution to the author(s) and the published article's title, journal citation, and DOI.

with an excitation energy comparable to, or higher than, the fission barrier. The populated state then undergoes fission in competition with other decay modes, such as  $\gamma$  decay and/or particle emission. The excitation energy of the daughter nucleus is limited by the  $Q_\beta$  value, which for known  $\beta$ DF cases is typically  $\lesssim 12$  MeV [2]. Therefore,  $\beta$ DF belongs to the so-called low-energy fission, which is sensitive to the underlying effects of nuclear structure. It allows for an investigation into the fission properties (e.g., partial half-lives and probabilities of  $\beta$ DF, fission fragment mass distributions, and respective total kinetic energies) of exotic isotopes for which low-energy fission studies by other, presently available approaches, are extremely difficult or impossible. As can be seen, for example, in Fig. 1 of Ref. [2],  $\beta$ DF measurements were employed for many exotic nuclei in the vicinity of the proton drip line in the lead and actinide regions. A noticeable example is the measurement of  $^{180}\text{Tl}$ , which led to an unexpected discovery of fully asymmetric fission of its  $\beta$ -decay daughter,  $^{180}\text{Hg}$  [3,4].

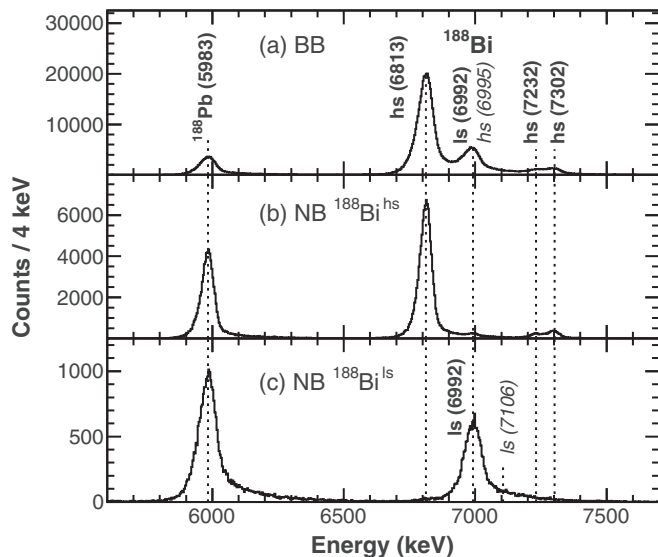


FIG. 1. Singles  $\alpha$ -decay spectra for different RILIS modes from Si1 and Si2 (only data from runs with wheel movement): (a) BB mode; (b) NB( $^{188}\text{Bi}^{\text{hs}}$ ) mode; and (c) NB( $^{188}\text{Bi}^{\text{ls}}$ ) mode.

All presently known cases of  $\beta$ DF occur in odd-odd isotopes [1]. These nuclei often possess two long-lived states with similar half-lives, both of which may decay via  $\beta$ DF [2]. For such cases, only  $\beta$ DF properties for a mixed sample containing nuclei of both states or upper limits of  $\beta$ DF probabilities for each state have been reported, as, e.g., for  $^{192,194}\text{At}$  [5],  $^{186,188}\text{Bi}$  [6], and  $^{202}\text{Fr}$  [7]. However, if these states could be studied separately, it may provide an opportunity to investigate the spin dependence of fission properties.

The present work is the first  $\beta$ DF study of separated isomeric states in one isotope. It focuses on  $^{188}\text{Bi}$ , for which  $\beta$ DF was first observed at Joint Institute for Nuclear Research (JINR), Dubna [8,9], where only one decaying state was identified. The most recent and comprehensive  $\alpha$ -decay and  $\beta$ DF study of  $^{188}\text{Bi}$  was performed at the velocity filter SHIP at GSI, Darmstadt [6,10]. Based on  $\alpha$ -decay measurements, two long-lived, presumably spherical, states with half-lives of 265(10) and 60(3) ms were observed with respective spin and parity assignments of  $I^\pi$  (high spin,  $^{188}\text{Bi}^{\text{hs}} = (10^-)$ ) and  $I^\pi$  (low spin,  $^{188}\text{Bi}^{\text{ls}} = (3^+)$ ) made by analogy with the heavier odd-odd bismuth isotopes [10]. As only four fission events were identified in the SHIP experiment [6], the authors could not assign them to a specific isomer. Therefore, an upper limit of  $\beta$ DF probability was evaluated for each isomer (using theoretical  $\beta$ -decay branching ratios):  $P_{\beta\text{DF}}(^{188}\text{Bi}^{\text{hs}}) \leq 1.6 \times 10^{-3}$  and  $P_{\beta\text{DF}}(^{188}\text{Bi}^{\text{ls}}) \leq 4.8 \times 10^{-3}$ .

Recently, based on in-source laser-spectroscopy measurements performed at the ISOLDE facility (Isotope Separator On Line Device) at CERN [11,12] by our collaboration, the near spherical nature and  $I^\pi = (10^-)$  assignment for  $^{188}\text{Bi}^{\text{hs}}$  were supported, while  $I^\pi = (1^+)$  was proposed as the most likely spin and parity for  $^{188}\text{Bi}^{\text{ls}}$  [13]. Moreover, based on the measured quadrupole moment and isotope shift, a strong prolate deformation of  $\beta_2 \approx 0.25$  was deduced for  $^{188}\text{Bi}^{\text{ls}}$ .

One of the important motivations for the present study is the fact that  $^{188}\text{Pb}$ , fissioning after the  $\beta$  decay of  $^{188}\text{Bi}$ , is located in a transitional region in the nuclear chart between nuclei with symmetric and asymmetric fission fragment mass distributions (FFMDs), as shown in Fig. 32 of Ref. [1]. Indeed, the low-energy fission of  $^{210}\text{Ra}$  and  $^{208,204}\text{Rn}$ , measured in relativistic Coulex experiments, exhibits a symmetric FFMD [14], while lighter nuclei  $^{196,194}\text{Po}$ , studied via  $\beta$ DF, have mixed symmetric and asymmetric FFMDs [7]. The even lighter isotope  $^{180}\text{Hg}$  exhibits a fully asymmetric FFMD [3,4]. The complexity of the FFMDs in this transitional region is demonstrated by the potential-energy surface (PES) calculations for the fission of  $^{196}\text{Po}$  [7,15]. The PES contains a broad, rather flat region without well pronounced fission valleys (in contrast to actinide nuclides [16]), and thus allows the occurrence of two or more fission modes. Therefore, fission studies in this region are particularly important for the investigation of the interplay between fission modes.

The present work reports on a study carried out at ISOLDE to investigate the  $\beta$ DF properties of  $^{188}\text{Bi}^{\text{hs,ls}}$  separately and to search for  $\beta$ DF of  $^{190}\text{Bi}$ , which has been unobserved so far. The results for  $^{188}\text{Bi}$  are compared to theoretical calculations within the Hartree-Fock-Bogolyubov (HFB) framework based on the DIM Gogny force [17] and within the quasiparticle random phase approximation (QRPA) [18].

## II. EXPERIMENT

Nuclei of  $^{188}\text{Bi}$  and  $^{190}\text{Bi}$  were produced in spallation reactions induced by 1.4-GeV protons impinging upon a thick  $\text{UC}_x$  target ( $50 \text{ g/cm}^2$ ). The proton beam with an intensity of up to  $2.1 \mu\text{A}$  was supplied by the Proton-Synchrotron Booster and was structured into 2.4- $\mu\text{s}$ -long pulses with a 1.2-s period. Pulses were grouped into the so-called supercycle, which typically consisted of around 30 pulses. The reaction products diffused through the target heated to  $\approx 2300 \text{ K}$  and effused via the heated transfer line into a hot cavity, where bismuth isotopes were selectively ionized by Resonance Ionization Laser Ion Source (RILIS) [19,20]. A three-step resonance ionization scheme using laser light with wavelengths of 306.9, 555.4, and 532 nm (the latter being nonresonant) [21] was applied. Different modes of the first-step laser operation were used during the measurement: broad bandwidth laser (BB mode, with a linewidth of  $\approx 14 \text{ GHz}$  for the 306.9-nm transition) was employed to ionize  $^{188}\text{Bi}$  or  $^{190}\text{Bi}$  atoms with nuclei in both the low- and high-spin isomeric states, while a narrow bandwidth laser with specific frequency (NB mode, with a linewidth of  $\approx 1.4 \text{ GHz}$  for the 306.9-nm transition) was applied to selectively ionize  $^{188}\text{Bi}$  atoms with nuclei in either the low- or the high-spin isomeric state, exploiting differences in their hyperfine structures [13]. The ions were accelerated to 30 keV and mass separated by the High Resolution Separator (HRS), which guaranteed a beam of ions with a mass of either  $A = 188$  or  $A = 190$  only, depending on the measured isotope.

After mass separation, the beam was implanted into one of ten thin ( $20 \mu\text{g/cm}^2$ ) carbon foils [22] mounted on a rotatable wheel in the Windmill detection system (WM) [3,23]. An annular silicon detector (Si1) with a 6-mm central hole (total area of  $450 \text{ mm}^2$  including the hole) to allow passage of

the beam was placed in front of the implantation foil. A circular silicon detector (Si2, area of 300 mm<sup>2</sup>) was mounted behind the foil. Both detectors were of surface-barrier type with a thickness of 300  $\mu$ m. In most cases, the WM wheel was rotated at the end of each supercycle to move the previously irradiated foil from the implantation position to the so-called decay position, between an additional pair of 300- $\mu$ m-thick PIPS silicon detectors (each with an area of 300 mm<sup>2</sup>). However, part of the measurement was performed without movement of the wheel in order to let <sup>188</sup>Pb decay at the implantation position in an attempt to deduce the  $\beta$ -decay branching ratio ( $b_\beta$ ) of <sup>188</sup>Bi (see Sec. IV A 1).

The energy calibration of silicon detectors was done separately for  $\alpha$  particles and for fission fragments (FFs). The main  $\alpha$ -decay transitions of <sup>188</sup>Bi<sup>hs</sup> (6813(5) keV), <sup>188</sup>Bi<sup>ls</sup> (6992(5) keV) [10], and <sup>188</sup>Pb (5983(4) keV) [24] were used for the  $\alpha$  calibration of the <sup>188</sup>Bi measurement. For the measurement of <sup>190</sup>Bi, energies of <sup>190</sup>Bi<sup>hs</sup> (6819(10) keV) [10] and <sup>190</sup>Pb (5581(4) keV) [24] were used.

The calibration for FFs was done for Si1 and Si2 according to the procedure described in detail in Refs. [4,25].<sup>1</sup> The procedure can only be used for events where coincident FFs were registered (i.e., both fragments from the same fission event were detected) and it requires some of the fission calibration parameters to be determined by dedicated measurement for each detector. These “fission parameters” are then scaled by the  $\alpha$ -decay calibration parameters used in other experiments in order to obtain the fission calibration for the specific experiment. Determination of the “fission parameters” was carried out at Institut Laue-Langevin (ILL, Grenoble) in 2011 for several detectors used in our experiments with WM. It was discovered that the detectors of the same type typically have almost the same “fission parameters” [25]. We used this finding, because the specific detectors employed in our experiment were not measured at ILL. For calibration of Si1 and Si2, we used the fission calibration parameters determined for another annular and circular surface-barrier detector, respectively.

Additional energy corrections are required for angle of impact on the detector, for energy losses in the carbon foil and because of different  $N/Z$  ratio of measured FFs compared to ions used for calibration at ILL. We used a correction for angle of impact for surface-barrier detectors from Ref. [25], where it was evaluated for the geometry at WM. The remaining two corrections were determined for  $\beta$ DF of <sup>180</sup>Tl in Ref. [4] and for  $\beta$ DF of <sup>202</sup>Fr in Ref. [25] (another experiment performed with WM at ISOLDE) and were within the uncertainties the same in both cases. Since our isotope of interest lies closer to <sup>180</sup>Tl, we used the values from Ref. [4]. The energy of the ion beam impinging on the carbon foil in these two earlier measurements was the same (30 keV) as in our study.

<sup>1</sup>It should be noted that we used corrected formulas in the procedure in the present study, due to minor errors in formulas in Ref. [25]: In Eq. (4.18), the first term in the calculation of parameter  $\alpha$  should be  $A_1'X_1$  instead of  $A_1'$  and the fourth term in the calculation of  $\beta$  should be  $B_2/F_2$  instead of  $B_2$ .

### III. PROBABILITY AND PARTIAL HALF-LIVES OF $\beta$ -DELAYED FISSION

The probability of  $\beta$ -delayed fission ( $P_{\beta\text{DF}}$ ) is defined as the ratio of the number of  $\beta$ DF events ( $N_{\beta\text{DF}}$ ) to the number of  $\beta$  decays. However, for predominantly  $\alpha$ -decaying nuclei it is useful to evaluate the partial  $\beta$ DF half-life as proposed in Ref. [2]:

$$T_{1/2p,\beta\text{DF}} = T_{1/2} \frac{N_{\text{dec,tot}}}{N_{\beta\text{DF}}}, \quad (1)$$

where  $T_{1/2}$  is the total half-life of the  $\beta$ DF precursor and  $N_{\text{dec,tot}}$  is the total number of its decays. In the cases when only FFs and  $\alpha$  decays are detected, while the  $\beta$ -decay branching ratio is small ( $b_\beta < 10\%$ ) and difficult to determine,  $T_{1/2p,\beta\text{DF}}$  can still be reliably evaluated using the approximation  $N_{\text{dec,tot}} \approx N_\alpha$  [2], where  $N_\alpha$  is the number of  $\alpha$  decays. We used this approximation to calculate the  $T_{1/2p,\beta\text{DF}}$  values shown in Table I.

In our experiment, FFs and  $\alpha$  particles were emitted from an external source and were measured by the same detectors. Since there are two FFs per one fission, the probability to detect singles FFs (i.e., individually counted FFs from Si1 and Si2 regardless as to whether they were in coincidence) from a given fission event is twice as high as the probability to detect an  $\alpha$  decay. Therefore,  $N_{\beta\text{DF}}$  in our calculations is defined as the number of singles FFs divided by two.

## IV. RESULTS AND DISCUSSIONS

### A. $\beta$ -delayed fission of <sup>188</sup>Bi

#### 1. Verification of isomer separation

To study  $\beta$ DF properties of the two isomers in <sup>188</sup>Bi separately, we exploited the difference in their hyperfine structures. Two different measurement modes, referred to as NB(<sup>188</sup>Bi<sup>hs</sup>) and NB(<sup>188</sup>Bi<sup>ls</sup>) mode, respectively, were employed by setting the NB laser frequency to selectively ionize either <sup>188</sup>Bi<sup>hs</sup> or <sup>188</sup>Bi<sup>ls</sup>. To confirm the separation of isomers in these modes, the  $\alpha$ -decay spectra were analyzed first (Fig. 1). In the BB measurement [Fig. 1(a)],  $\alpha$ -decay peaks from both isomers were present. The observed high-spin to low-spin isomer ratio based on  $\alpha$  decays<sup>2</sup> was 75(1)% : 25(1)%.

In the NB(<sup>188</sup>Bi<sup>hs</sup>) mode shown in Fig. 1(b), in addition to the 6813-keV  $\alpha$ -decay peak of <sup>188</sup>Bi<sup>hs</sup>, there are three known fine-structure  $\alpha$  decays; the energies of these transitions were reported in Ref. [10] at 6995(15), 7232(10), and 7302(5)

<sup>2</sup>The contribution of the 6995-keV fine-structure decay from <sup>188</sup>Bi<sup>hs</sup> in the 6992-keV peak of <sup>188</sup>Bi<sup>ls</sup> was corrected for by using the number of  $\alpha$  decays in the 6813-keV peak of <sup>188</sup>Bi<sup>hs</sup> and relative intensity of 1.5(5)% for the 6995-keV decay from Ref. [10].

TABLE I. Time of the data collection in hours ( $T$ ) and values extracted from BB and NB mode measurements: number of singles  $\alpha$  decays ( $N_\alpha$ ), singles FFs ( $N_{\text{FF}}$ ), FF coincidences ( $N_{\text{FFC}}$ ), ratio of number of fission events and  $\alpha$  decays ( $N_{\beta\text{DF}}/N_\alpha$ ), partial half-lives of  $\beta\text{DF}$  ( $T_{1/2p,\beta\text{DF}}$ ), theoretical  $\beta$ -decay branching ratios ( $b_{\beta,\text{th}}$ ) and probabilities of  $\beta\text{DF}$  ( $P_{\beta\text{DF}}$ ). The  $b_{\beta,\text{th}}$  values used to calculate  $P_{\beta\text{DF}}$  are based on experimental half-lives of isomers from Ref. [10] and on DIM+QRPA estimates of the  $\beta$ -decay rates from Table III; see Sec. V for details. In the case of  $^{188}\text{Bi}^{\text{ls}}$ , a range of these estimates for prolate  $I^\pi = 1^+$  states, compatible with experimental  $T_{1/2p,\beta\text{DF}}$ , was used. Because of the large uncertainties for NB( $^{188}\text{Bi}^{\text{ls}}$ ) and wide range of  $b_{\beta,\text{th}}$ , we give only range of orders of magnitude for corresponding  $P_{\beta\text{DF}}$  value.

NB and BB data separately								
Laser mode	$T$ (h)	$N_\alpha$	$N_{\text{FF}}$	$N_{\text{FFC}}$	$N_{\beta\text{DF}}/N_\alpha$	$T_{1/2p,\beta\text{DF}}$ (s)	$b_{\beta,\text{th}}$ (%)	$P_{\beta\text{DF}}^{\text{a}}$
NB( $^{188}\text{Bi}^{\text{hs}}$ )	7.1	$1.24 \times 10^5$	12	5	$4.8(14) \times 10^{-5}$	$5.5(16) \times 10^3$	1	$4.7(13) \times 10^{-3}$
NB( $^{188}\text{Bi}^{\text{ls}}$ )	3.9	$5.42 \times 10^4$	2	0	$1.8^{+2.4}_{-1.2} \times 10^{-5}$	$3.3^{+5.9}_{-1.9} \times 10^3$	2–8	$10^{-4}$ – $10^{-3}$
BB	7.8	$1.04 \times 10^6$	104	31	$5.0(5) \times 10^{-5}$	$4.3(5) \times 10^3$		
Combination of NB and time-gated BB data								
Isomer	$N_\alpha$	$N_{\text{FF}}$	$N_{\beta\text{DF}}/N_\alpha$	$T_{1/2p,\beta\text{DF}}$ (s)	$b_{\beta,\text{th}}$ (%)	$P_{\beta\text{DF}}^{\text{a}}$		
$^{188}\text{Bi}^{\text{hs}}$	$5.45 \times 10^5$	52	$4.8(8) \times 10^{-5}$	$5.6(8) \times 10^3$	1	$4.6(9) \times 10^{-3}$		
$^{188}\text{Bi}^{\text{ls}}$	$1.9(2) \times 10^{5\text{b}}$	14(5)	$3.6(14) \times 10^{-5}$	$1.7(6) \times 10^3$	2–8	$0.4(2)$ – $1.8(7) \times 10^{-3}$		

<sup>a</sup>Only the statistical uncertainty from the measurement is shown. However, an additional uncertainty of factor of 3 comes from the theoretical  $b_{\beta,\text{th}}$  values used; see Sec. V for details.

<sup>b</sup>A mixture of  $^{188}\text{Bi}^{\text{hs}}$  and  $^{188}\text{Bi}^{\text{ls}}$  was present in this time gate; the uncertainty stems from the deconvolution of the  $\alpha$ -decay spectrum (Fig. 4).

keV, respectively. The peak at 6995 keV is strongly reduced compared to the BB spectrum [Fig. 1(a)], since there it was predominantly formed by the main  $\alpha$  decay of  $^{188}\text{Bi}^{\text{ls}}$  (with a similar energy of 6992(5) keV [10]). In contrast, the dominant  $\alpha$  decay belonging to  $^{188}\text{Bi}$  in the NB( $^{188}\text{Bi}^{\text{ls}}$ ) spectrum [Fig. 1(c)] is the 6992-keV decay from  $^{188}\text{Bi}^{\text{ls}}$ , while the 6813-keV peak from  $^{188}\text{Bi}^{\text{hs}}$  seems to be absent.

To evaluate the possibility of a small admixture of the other isomer in each NB mode setting, due to the finite linewidth of the laser, we used differences in the half-lives of the isomers. The distributions in the time differences ( $\Delta t$ ) between proton pulse impacts on the target and subsequent  $\alpha$  decays in the WM for the two isomers are significantly different (Fig. 2). It

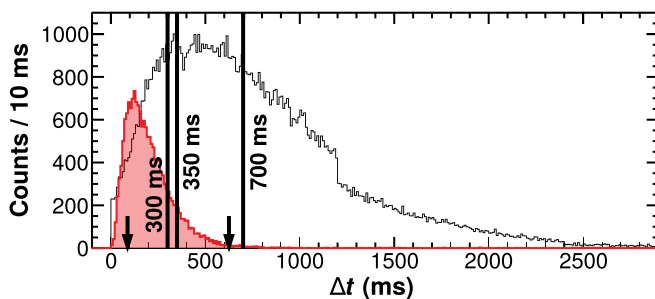


FIG. 2. Number of  $\alpha$  decays of  $^{188}\text{Bi}^{\text{hs}}$  (black) and  $^{188}\text{Bi}^{\text{ls}}$  (red, shaded) as a function of time differences ( $\Delta t$ ) between time of  $\alpha$  decay in the Si1 or Si2 and the last preceding proton pulse on the HRS target. Spectra were produced from NB runs with WM movement. Vertical lines show specific times used for gating in data analysis; see text for details. Time values for the two fission events from NB( $^{188}\text{Bi}^{\text{ls}}$ ) mode are marked by arrows. The “jump” at 1.2 s is caused by the 1.2-s period of the proton pulses—if two consecutive pulses arrived on the HRS target, only  $\Delta t$  up to 1.2 s can be determined for decays after the first pulse.

should be noted that these time distributions are combinations of release curves from the target and decay curves.

For data collected in the NB( $^{188}\text{Bi}^{\text{hs}}$ ) mode [Fig. 1(b)], the intensity of the 6995-keV peak relative to the 6813-keV  $\alpha$  decay of  $^{188}\text{Bi}^{\text{hs}}$  was found to be  $I_{\text{rel}}(6995 \text{ keV}) = 0.66(8)\%$ . Note that in the case of an admixture between states, this intensity would include contribution from the 6992-keV decay of  $^{188}\text{Bi}^{\text{ls}}$ . If we select only events with  $\Delta t \geq 700$  ms, for which 99% of  $^{188}\text{Bi}^{\text{ls}}$  is already decayed according to the distribution in Fig. 2, the intensity is  $I_{\text{rel}}(6995 \text{ keV}) = 0.59(11)\%$ . Within the uncertainty, this intensity is the same as for the whole NB( $^{188}\text{Bi}^{\text{hs}}$ ) data set, which suggests negligible (on the level of  $I_{\text{rel}} \approx 0.1\%$ ) or no contribution from  $^{188}\text{Bi}^{\text{ls}}$ . We note that our  $I_{\text{rel}}(6995 \text{ keV})$  value is lower than the value of 1.5(5)% from Ref. [10]. The difference is most likely caused by  $\alpha +$  conversion electron summing, since as discussed in Ref. [10], the 6995-keV transition is followed by highly converted 70.5-keV  $\gamma$  decay. Thus, when the 6995-keV  $\alpha$  particle hits the same detector as the subsequent conversion electron, their signals will be summed and detected energy will be shifted outside of the 6995-keV peak.

In the NB( $^{188}\text{Bi}^{\text{ls}}$ ) measurement [Fig. 1(c)], the 6992-keV  $\alpha$ -decay peak of  $^{188}\text{Bi}^{\text{ls}}$  has high- and low-energy tails. A small part of the high-energy tail stems from the  $E_\alpha = 7106(5)$  keV ( $I_{\text{rel}} = 2.1(2)\%$ ) fine-structure  $\alpha$  decay of  $^{188}\text{Bi}^{\text{ls}}$  and from the  $\alpha +$  conversion electron summing peak at 7028(10) keV, both reported in Ref. [10]. The dominant part of the high-energy tail and broadening of the 6992-keV peak is caused by random summing with  $\beta$  particles and conversion electrons following  $\beta$  decays of long-lived contaminants present due to ionization independent of lasers ( $^{188}\text{Pb}$  and mostly surface-ionized  $^{188}\text{Tl}$  decaying to  $^{188}\text{Hg}$ ).

To evaluate possible admixture of  $^{188}\text{Bi}^{\text{hs}}$  in the low-energy tail of the 6992-keV peak in Fig. 1(c), we again selected events with time differences  $\Delta t \geq 700$  ms. For these events, the part

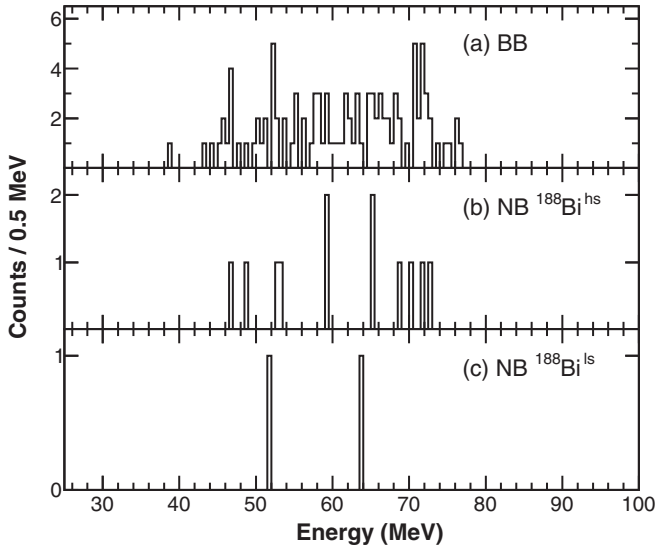


FIG. 3. Singles FF spectra from Si1 and Si2 for different RILIS modes: (a) BB mode; (b) NB( $^{188}\text{Bi}^{\text{hs}}$ ) mode; and (c) NB( $^{188}\text{Bi}^{\text{ls}}$ ) mode. Only calibration based on  $\alpha$  decays is used as a rough calibration, without any additional corrections; see text for details.

of the low-energy tail stemming directly from the main  $^{188}\text{Bi}^{\text{ls}}$   $\alpha$  decay was reduced and from the remaining decays we could then evaluate the admixture of  $^{188}\text{Bi}^{\text{hs}}$  in the NB( $^{188}\text{Bi}^{\text{ls}}$ ) to be  $N_{\alpha}(^{188}\text{Bi}^{\text{hs}})/N_{\alpha}(^{188}\text{Bi}^{\text{ls}}) = 1.1(2)\%$ .

The experimental  $b_{\beta}$  values of  $^{188}\text{Bi}^{\text{hs,ls}}$  are not known, but they are expected to be small (below 10%), which is supported by the theoretical estimates in Table I. As an attempt to deduce  $b_{\beta}$  experimentally, we performed part of the measurement in the mode without movement of the WM wheel to let  $^{188}\text{Pb}$  fully decay at the implantation position ( $T_{1/2}(^{188}\text{Pb}) = 25.5(1)$  s [26]). However, the contribution of  $^{188}\text{Pb}$  coming directly from the ion source (not laser-ionized) was so high that even relatively small fluctuations in its direct production rate made it impossible to resolve a small increase in its total production caused by the  $\beta$  decay of  $^{188}\text{Bi}$ . Strong direct production of  $^{188}\text{Pb}$  was confirmed by measurement with the lasers switched off, where the production rate did not change significantly and systematically compared to the measurement with lasers switched on. Abundant presence of directly produced  $^{188}\text{Pb}$  is also visible in Fig. 1 (we note that  $\alpha$ -decay branching ratio of  $^{188}\text{Pb}$  is only  $b_{\alpha} = 9.3(8)\%$  [27]).

### 2. NB and BB mode results separately

The energy distribution of singles FFs from BB data, containing 104 events, is shown in Fig. 3(a). The shape of the spectrum, without any indication of a central peak, is a hint that an asymmetric mass split plays a substantial role in the corresponding FFMD.<sup>3</sup> The singles FFs from NB( $^{188}\text{Bi}^{\text{hs}}$ )

and NB( $^{188}\text{Bi}^{\text{ls}}$ ) modes are presented in Figs. 3(b) and 3(c), respectively.

As a first step, we determined  $T_{1/2p,\beta\text{DF}}$  and  $P_{\beta\text{DF}}$  values from NB measurements with clean samples for both isomers (this section). Afterward, in Sec. IV A 3, we used time gating to partially separate the isomers in BB mode and then combined extracted statistics with NB mode data to obtain more precise, final results.

In Sec. IV A 1, we established that the admixture of  $^{188}\text{Bi}^{\text{ls}}$  in NB( $^{188}\text{Bi}^{\text{hs}}$ ) mode is negligible, therefore we assigned all 12 FFs registered in NB( $^{188}\text{Bi}^{\text{hs}}$ ) mode [Fig. 3(b)] to  $\beta\text{DF}$  of  $^{188}\text{Bi}^{\text{hs}}$ . The extracted results including  $P_{\beta\text{DF}}$  values evaluated using theoretical  $b_{\beta,\text{th}}$  are summarized in the upper part of Table I.

For NB( $^{188}\text{Bi}^{\text{ls}}$ ) mode, we determined in Sec. IV A 1 that the admixture of  $^{188}\text{Bi}^{\text{hs}}$   $\alpha$  decays is 1.1(2)%. Based on this value and the ratio of the number of fission events to  $N_{\alpha}(^{188}\text{Bi}^{\text{hs}})$  deduced from NB( $^{188}\text{Bi}^{\text{hs}}$ ) mode (Table I), the expected number of singles FFs from the  $^{188}\text{Bi}^{\text{hs}}$  admixture is only 0.06(2). Moreover, for the two FFs detected in NB( $^{188}\text{Bi}^{\text{ls}}$ ) mode [Fig. 3(c)], the time differences between the registration of FF and the previous proton pulse were 88 and 625 ms. These values are compared in Fig. 2 to time distributions of  $\alpha$  decays for both isomers measured in NB mode. The 88-ms value is almost at the maximum of  $^{188}\text{Bi}^{\text{ls}}$  time distribution (shaded histogram in Fig. 2) and the 625-ms value is in the area where most of the  $^{188}\text{Bi}^{\text{ls}}$  has already decayed. However, since the admixture of  $^{188}\text{Bi}^{\text{hs}}$  in NB( $^{188}\text{Bi}^{\text{ls}}$ ) is very small, at 625 ms the ratio of  $N_{\alpha}(^{188}\text{Bi}^{\text{hs}})/N_{\alpha}(^{188}\text{Bi}^{\text{ls}})$  is  $\lesssim 0.5$ , and considering the  $b_{\beta,\text{th}}$  values in Table I, the difference in  $\beta$ -decay rate should be even more in favor of  $^{188}\text{Bi}^{\text{ls}}$ . Therefore, we assigned both fission events to the  $\beta\text{DF}$  of  $^{188}\text{Bi}^{\text{ls}}$ . Deduced values from NB( $^{188}\text{Bi}^{\text{ls}}$ ) and also from the full data set from BB mode are listed in the upper part of Table I.

### 3. Combination of NB and time-gated BB mode results

As can be seen in Fig. 3 and the upper part of Table I, most of the statistics were collected during BB mode. Although both isomers were delivered simultaneously to our detection system in this mode, we can partially separate them by time gating on the differences between proton pulse and subsequent decay times, similar to the procedure described in Sec. IV A 1 for the analysis of  $\alpha$  decays (Fig. 2). To specifically focus on the longer lived ( $^{188}\text{Bi}^{\text{hs}}$ ) and shorter lived ( $^{188}\text{Bi}^{\text{ls}}$ ) isomer and thus to extract their  $\beta\text{DF}$  properties, we used time gates of  $\Delta t \geq 700$  ms and  $\Delta t \leq 300$  ms, respectively. Corresponding time-gated  $\alpha$ -decay spectra are presented in Fig. 4.

Based on distributions in Fig. 2, only  $\approx 1\%$  of all  $^{188}\text{Bi}^{\text{ls}}$   $\alpha$  decays occur above 700 ms, while there are still  $\approx 47\%$  of all  $^{188}\text{Bi}^{\text{hs}}$   $\alpha$  decays. Considering also the production ratio of the isomers in BB mode and  $N_{\beta\text{DF}}/N_{\alpha}$  ratios from NB( $^{188}\text{Bi}^{\text{ls}}$ ) and NB( $^{188}\text{Bi}^{\text{hs}}$ ), the expected contribution of  $\beta\text{DF}$  from  $^{188}\text{Bi}^{\text{ls}}$  in the given time gate is 0.1(1) FF. Therefore, we assigned

<sup>3</sup>In the detection system consisting of two detectors positioned on opposite sides of the implantation foil, each detector may register only one FF from a specific event. Because of linear momentum con-

servation, the kinetic energies of the FFs are inversely proportional to their masses. Therefore, a symmetric mass split would result in an energy distribution containing one peak.

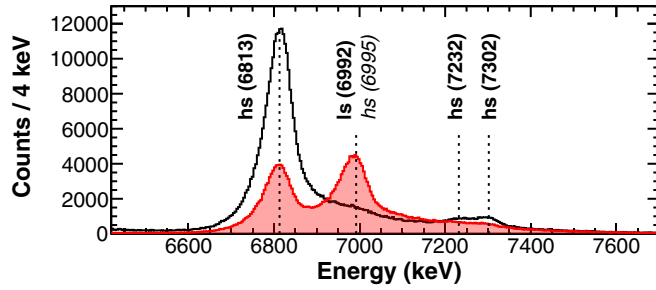


FIG. 4. Time-gated  $\alpha$ -decay spectra from BB measurements from Si1 and Si2: For differences between proton pulse times and decay times  $\Delta t \geq 700$  ms (black histogram) and  $\Delta t \leq 300$  ms (red, shaded histogram).

all 40 FFs present within  $\Delta t \geq 700$  ms in BB mode to the  $\beta$ DF of  $^{188}\text{Bi}^{\text{hs}}$ . By combining these FFs with the data from the NB( $^{188}\text{Bi}^{\text{hs}}$ ) measurement, we obtained final statistics of 52 FFs. The resulting values of  $T_{1/2p,\beta\text{DF}}$  and  $P_{\beta\text{DF}}$  for  $^{188}\text{Bi}^{\text{hs}}$  shown in the lower part of Table I are almost the same as from NB( $^{188}\text{Bi}^{\text{hs}}$ ) mode only, but more precise.

Similarly, we employed time gating to select additional fission events for  $^{188}\text{Bi}^{\text{ls}}$ . For events with time differences  $\Delta t \leq 300$  ms, the relative contribution of  $^{188}\text{Bi}^{\text{ls}}$  is increased compared to the whole data set. Within this time gate, there are 22 FFs,  $\approx 81\%$  of all  $^{188}\text{Bi}^{\text{ls}}$   $\alpha$  decays and only  $\approx 15\%$  of all  $^{188}\text{Bi}^{\text{hs}}$   $\alpha$  decays. The contribution of fissions from  $\beta$ DF of  $^{188}\text{Bi}^{\text{hs}}$  was estimated based on the number of  $^{188}\text{Bi}^{\text{hs}}$   $\alpha$  decays within the time gate and the  $N_{\beta\text{DF}}/N_{\alpha}(^{188}\text{Bi}^{\text{hs}})$  ratio determined from the analysis above. After subtraction of this contribution and addition of the two FFs from NB( $^{188}\text{Bi}^{\text{ls}}$ ) mode, we obtained 14(5) FFs. The final results for  $^{188}\text{Bi}^{\text{ls}}$  are shown in the lower part of Table I. There is almost a factor of two difference in the  $T_{1/2p,\beta\text{DF}}$  and  $P_{\beta\text{DF}}$  values compared to the results from NB( $^{188}\text{Bi}^{\text{ls}}$ ) mode only, but they are consistent within uncertainties. The shorter final  $T_{1/2p,\beta\text{DF}}$  (and thus higher fission rate) than the value from NB( $^{188}\text{Bi}^{\text{ls}}$ ) mode alone supports our assignment of both FFs from NB( $^{188}\text{Bi}^{\text{ls}}$ ) to  $\beta$ DF of  $^{188}\text{Bi}^{\text{ls}}$ .

The final  $T_{1/2p,\beta\text{DF}}(^{188}\text{Bi}^{\text{hs,ls}})$  values are plotted alongside other  $\beta$ DF partial half-lives in the neutron-deficient region as a function of differences between  $Q_{\beta}$  values and fission barrier heights ( $B_f$ ) in Fig. 5. As recognized already in Refs. [2,31], the  $\log_{10}(T_{1/2p,\beta\text{DF}})$  values show a linear dependence on difference  $Q_{\beta} - B_f$  for a broad range of isotopes. In particular, in Fig. 5 the isotopes span from  $^{178}\text{Tl}$  up to  $^{250}\text{Md}$  (when sorted by mass). The  $T_{1/2p,\beta\text{DF}}(^{188}\text{Bi}^{\text{hs}})$  fits quite well into this systematics, while the  $T_{1/2p,\beta\text{DF}}(^{188}\text{Bi}^{\text{ls}})$  is somewhat on the lower side but still consistent with the general trend. Similarly, the final  $P_{\beta\text{DF}}$  values for both isomers fit into analogous systematics of  $\beta$ DF probabilities (shown for example in Ref. [32]).

The partial half-lives of  $\beta$ DF of  $^{188}\text{Bi}^{\text{hs,ls}}$  are also consistent with the lower limits on  $T_{1/2p,\beta\text{DF}}$  extracted from the results given in Ref. [6]:  $T_{1/2p,\beta\text{DF}}(^{188}\text{Bi}^{\text{hs}}) \geq 3.4 \times 10^3$  s and  $T_{1/2p,\beta\text{DF}}(^{188}\text{Bi}^{\text{ls}}) \geq 1.1 \times 10^3$  s. In the earlier study [34],  $P_{\beta\text{DF}} = 3.4 \times 10^{-4}$  with an uncertainty of a factor of four was reported, based on the estimated  $b_{\beta} = 2.4\%$  and the

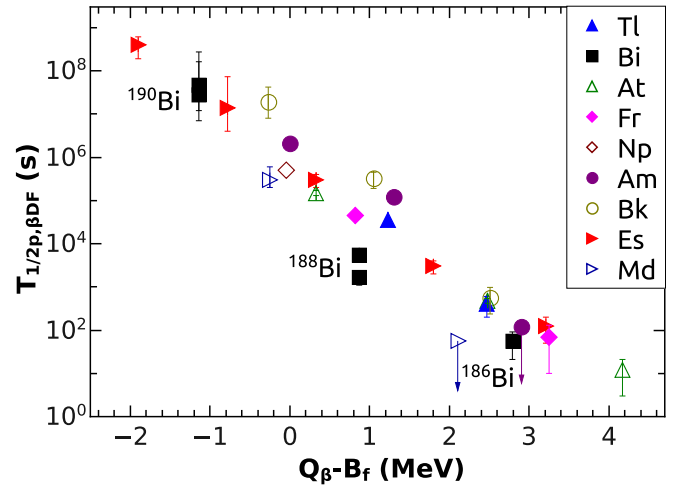


FIG. 5. Systematics of  $T_{1/2p,\beta\text{DF}}$  values in the neutron-deficient region including our results for  $^{188}\text{Bi}$  and  $^{190}\text{Bi}$  (see Secs. IV A 3 and IV B for details), as a function of difference  $Q_{\beta} - B_f$ . The electron-capture decay  $Q$  values from Ref. [28] were used for  $Q_{\beta}$ . The  $B_f$  values are from Thomas-Fermi model [29] with microscopic (shell) corrections from FRDM [30]. Literature values of  $T_{1/2p,\beta\text{DF}}$  were taken from Ref. [31] and in the case of  $^{230}\text{Am}$ ,  $^{236}\text{Bk}$ , and  $^{240}\text{Es}$ , they were calculated based on  $P_{\beta\text{DF}}$ ,  $b_{\beta}$ , and  $T_{1/2}$  values given in Refs. [32,33]. We note that the data points were larger than the error bar range for several cases in the figure. Downward arrow indicates that the value is an upper limit.

experimental results on  $\beta$ DF from Refs. [8,9]. No distinction between the isomers in  $^{188}\text{Bi}$  could be done and only one half-life of 0.21(9) s was considered at the time [34]. Based on these values, a partial half-life  $T_{1/2p,\beta\text{DF}} = 2.6 \times 10^4$  s can be deduced. This value is several times higher than our results for both isomers and than the limits extracted from the results in Ref. [6].

#### 4. Total kinetic energy and FFMD for $\beta$ DF of $^{188}\text{Bi}^{\text{hs}}$

To deduce the total kinetic energy and the FF mass distribution, we needed to select FF coincidences (see Sec. II) for a specific isomer. Analysis of BB mode data in Sec. IV A 3 showed that this was possible for  $^{188}\text{Bi}^{\text{hs}}$  by using time gating. Because of the low statistics, the applied condition was less strict ( $\Delta t \geq 350$  ms) than for the evaluation of  $T_{1/2p,\beta\text{DF}}$ . With this condition, only 12.4% of  $^{188}\text{Bi}^{\text{ls}}$   $\alpha$  decays are included, while 78% remain for  $^{188}\text{Bi}^{\text{hs}}$ . There were 24 FF coincidences within this time gate in BB mode. Two additional FF coincidences fulfilling the time condition were registered during laser optimization and laser-spectroscopy runs and were included in the analysis. Based on the observed isomer ratio,  $N_{\beta\text{DF}}/N_{\alpha}$  ratios, and the time behavior of both isomers, we estimated that 96(2)% of these 26 FF coincidences belonged to  $\beta$ DF of  $^{188}\text{Bi}^{\text{hs}}$ . Finally, we added 5 FF coincidences from NB( $^{188}\text{Bi}^{\text{hs}}$ ) mode and obtained a sample of 31 coincident  $\beta$ DF events.

We applied the fission calibration procedure described in Sec. II on these selected 31 events. The procedure includes an iterative correction on the fragment's kinetic energy carried

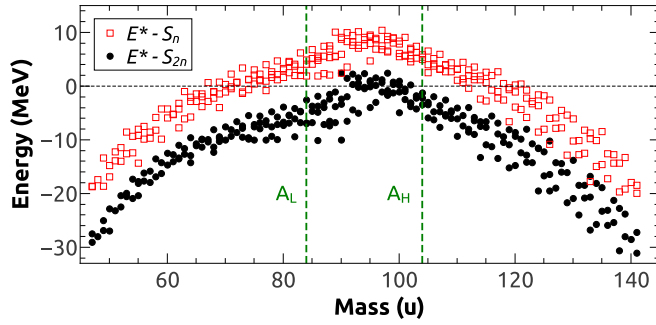


FIG. 6. Excitation energies for possible individual fission fragments after subtraction of one-neutron (open red squares) and two-neutron (black circles) separation energies. Experimental mean masses of light and heavy fragments are marked as  $A_L$  and  $A_H$ . For more details, see text.

away by emitted prompt neutrons. The first iteration was done assuming no prompt neutron emission. We would like to note that since this energy correction is relatively small, only the final spectra are shown below. From the first iteration, it was deduced that the FFMD has an asymmetric component and approximate mean masses of light and heavy fragments were determined. Mean total kinetic energy (TKE) was evaluated as well and then an estimate of the number of prompt neutrons was made in a similar way as in Refs. [4,25]. We evaluated the excitation energies of possible FFs with a similar  $N/Z$  ratio ( $\approx 1.29$ ) as the fissioning isotope  $^{188}\text{Pb}$  (assuming an equal distribution of excitation energy between both fragments):

$$E^* = \frac{Q - E_{\text{tot.,kin}}}{2}, \quad (2)$$

where  $E_{\text{tot.,kin}}$  denotes  $\overline{\text{TKE}}$  and  $Q$  values were based on masses from Ref. [28]. The one- ( $S_n$ ) and two- ( $S_{2n}$ ) neutron separation energies (taken from Ref. [28]) were then subtracted from the excitation energies for specific fragments; the results are shown in Fig. 6.

Final  $E^*$  values after subtraction of  $S_n$  are positive in the vicinity of expected fragment masses, while most of the values after subtraction of  $S_{2n}$  are negative. Based on the above it can be concluded that the emission of one prompt neutron per FF, i.e., two neutrons per fission, is most likely. However, since some of the values after subtraction of  $S_{2n}$  are still positive and since the excitation energy may not be distributed exactly equally between the fragments, the average number of emitted prompt neutrons per fission may be between 2 and 3.

The resulting pre-neutron-emission FFMD calibrated with the assumption of two emitted prompt neutrons per fission is presented in Fig. 7(a). A single symmetric FFMD is excluded based on the wide flat-topped distribution in the range of 79–109 u. However, the spectrum can be explained by a mixture of symmetric and asymmetric fission modes. To explore this option, we fitted the data with three Gaussians, where the width of the peak corresponding to the symmetric mode was left as a free parameter and the widths of the peaks corresponding to the asymmetric mode were fixed to a full width at half maximum of  $\text{FWHM} = 10.9$  u. This FWHM value was deduced for the FFMD peaks from the  $\beta\text{DF}$  of  $^{180}\text{Tl}$  measured

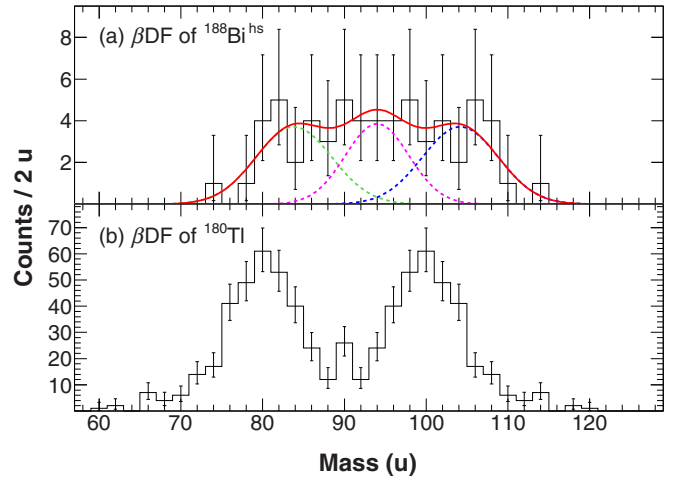


FIG. 7. Pre-neutron-emission FFMDs: (a) for  $\beta\text{DF}$  of  $^{188}\text{Bi}^{\text{hs}}$  (this work); (b) for  $\beta\text{DF}$  of  $^{180}\text{Tl}$  [4], rebinned in the same way as in panel (a). Red solid curve in panel (a) shows a fit corresponding to mixed symmetric and asymmetric FFMD; dashed curves show components of the fit.

with the WM [4]; the corresponding spectrum is shown in Fig. 7(b) for comparison with the results from the current experiment. The resulting mean values of Gaussians from the fit [Fig. 7(a)] were 84(2), 94(2), and 104(2) u, respectively, and the FWHM of the symmetric component was 9(4) u. Assuming the same  $N/Z$  ratio for FFs as for  $^{188}\text{Pb}$ , the most probable FFs would be around  $^{84}_{37}\text{Rb}_{47}$ ,  $^{94}_{41}\text{Nb}_{53}$ , and  $^{104}_{45}\text{Rh}_{59}$ . The contribution of the symmetric mass split is  $\approx 30\%$  under applied fitting conditions.

The deduced mixture of two fission modes is consistent with the placement of  $^{188}\text{Pb}$  in the transitional region in the nuclear chart between nuclei with predominantly symmetric and asymmetric fission modes. Interestingly, the separation of mean values of the asymmetric component is 20 u, which is the same value as for  $\beta\text{DF}$  of  $^{180}\text{Tl}$  [Ref. [4] and Fig. 7(b)] and for the asymmetric component in  $\beta\text{DF}$  of  $^{196}\text{At}$  [35].

The distribution of the total kinetic energies of the selected 31 coincident  $\beta\text{DF}$  events is shown in Fig. 8. Because of the low statistics, it was not possible to reliably distinguish two components in the measured distribution (corresponding to two FFMD modes), and thus we report a mean value of

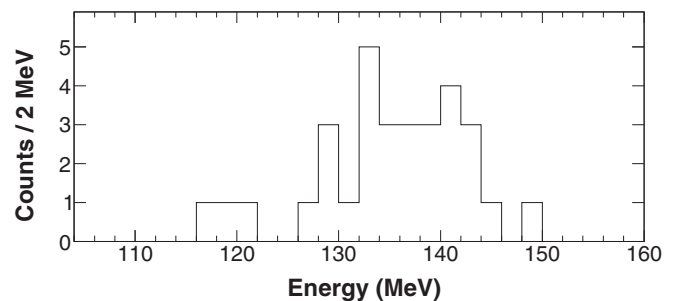


FIG. 8. Distribution of TKE for 31 selected events for  $\beta\text{DF}$  of  $^{188}\text{Bi}^{\text{hs}}$ , calibrated with the assumption of two prompt neutrons emitted per fission.

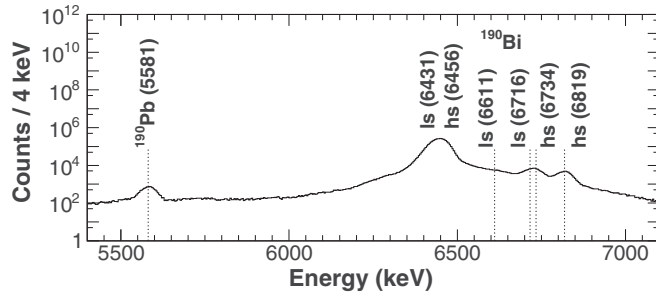


FIG. 9. Singles  $\alpha$ -decay spectrum from  $^{190}\text{Bi}$  measurement from all four silicon detectors.

the whole spectrum:  $\overline{\text{TKE}} = 135.1(19)$  MeV (a correction for the emission of two prompt neutrons per fission event was applied; the correction results in an increase of  $\overline{\text{TKE}}$  by  $\approx 0.65$  MeV per neutron).

### B. $\beta$ -delayed fission of $^{190}\text{Bi}$

We performed a short ( $\approx 45$  min) BB measurement of  $^{190}\text{Bi}$  in order to search for its  $\beta\text{DF}$  and we registered one FF with an energy of 74 MeV (using an  $\alpha$ -decay calibration). Since there is no possible contamination at mass  $A = 190$  which could decay via spontaneous or  $\beta$ -delayed fission, the registered FF represents the first observation of  $\beta\text{DF}$  for  $^{190}\text{Bi}$ .

Two long-lived  $\alpha$ -decaying states are known in  $^{190}\text{Bi}$  with suggested spin and parity assignments of  $I^\pi$  (high spin,  $^{190}\text{Bi}^{\text{hs}} = (10^-)$ ,  $I^\pi$  (low spin,  $^{190}\text{Bi}^{\text{ls}} = (3^+)$ ) and half-lives of 5.9(6) s and 5.7(8) s, respectively [10]. Both isomers were delivered to the WM setup simultaneously during the measurement.

The energies of the main  $\alpha$  decays of the isomers were reported to be 6456(5) keV ( $^{190}\text{Bi}^{\text{hs}}$ ) and 6431(10) keV ( $^{190}\text{Bi}^{\text{ls}}$ ) [10] and could not be resolved in our experiment (Fig. 9). Therefore, the number of  $\alpha$  decays of the respective isomer was estimated using known, relatively strong, fine-structure  $\alpha$  decays and their relative intensities from Ref. [10]:  $E_\alpha = 6734(10)$  keV,  $I_\alpha = 1.5(2)\%$  and  $E_\alpha = 6819(10)$  keV,  $I_\alpha = 2.0(3)\%$  for  $^{190}\text{Bi}^{\text{hs}}$ , and  $E_\alpha = 6716(10)$  keV,  $I_\alpha = 1.5(2)\%$  and  $E_\alpha = 6611(10)$  keV,  $I_\alpha = 2.2(3)\%$  for  $^{190}\text{Bi}^{\text{ls}}$ . Using these values together with the number of counts in the 6819-keV peak and the common peak of the 6716- and 6734-keV decays in Fig. 9, it was possible to determine that the ratio of the number of  $\alpha$  decays from the high-spin isomer to the number of  $\alpha$  decays from the low-spin isomer was 56(8)% : 44(8)% in our experiment. The 6611-keV decay could not be resolved in our data due to the large high-energy tail from the  $\approx 6440$ -keV peak, but its relative intensity from Ref. [10] was taken into account in evaluation of this  $\alpha$ -decay ratio. In the whole energy range of  $^{190}\text{Bi}$   $\alpha$  decays, there were  $5 \times 10^6$  counts, which we divided according to the deduced  $\alpha$ -decay ratio in order to determine the number of counts from each isomer, given in Table II.

The observed FF could not be attributed to a specific isomer, and therefore we calculated  $T_{1/2p, \beta\text{DF}}$  values (Table II) for each isomer as if the FF originated from its  $\beta\text{DF}$  decay. For the isomer which was not the precursor of the fission event,

TABLE II. BB measurement of  $^{190}\text{Bi}$ : number of singles  $\alpha$  decays ( $N_\alpha$ ),  $\alpha$ -decay branching ratios ( $b_\alpha$ ), and partial half-lives of  $\beta\text{DF}$  ( $T_{1/2p, \beta\text{DF}}$ ).  $N_{\text{FF}}$  denotes the number of FFs used to evaluate  $T_{1/2p, \beta\text{DF}}$ . Only one FF was observed in the measurement and it originated from  $\beta\text{DF}$  of either  $^{190}\text{Bi}^{\text{hs}}$  or  $^{190}\text{Bi}^{\text{ls}}$ . The stated  $T_{1/2p, \beta\text{DF}}$  value is thus valid only for the isomer, which is the precursor of the fission event, while for the other isomer it serves as a lower limit.

Isomer	$N_\alpha$	$N_{\text{FF}}$	$b_\alpha$ (%) [10]	$T_{1/2p, \beta\text{DF}}$ (s)
$^{190}\text{Bi}^{\text{hs}}$	$2.8(4) \times 10^6$	1	70(9)	$4.7^{+22.6}_{-3.5} \times 10^7$
$^{190}\text{Bi}^{\text{ls}}$	$2.2(4) \times 10^6$	1	$90^{+10}_{-30}$	$2.8^{+13.4}_{-2.1} \times 10^7$

the value represents a lower limit of  $T_{1/2p, \beta\text{DF}}$ . The results for  $^{190}\text{Bi}$  fit well into the systematics of  $\beta\text{DF}$  partial half-lives (Fig. 5).

## V. COMPARISON WITH THEORY

### A. Theoretical $P_{\beta\text{DF}}$ and $T_{1/2p, \beta\text{DF}}$ values

HFB calculations were performed to study the spectroscopic properties of  $^{188}\text{Bi}$  on the basis of the DIM Gogny interaction [17]. Since  $^{188}\text{Bi}$  is an odd-odd nucleus, the so-called equal filling approximation, keeping time-reversal symmetry, was applied to estimate the binding energy. The lowest energy was defined in each case by blocking the various possible levels around the Fermi energy.

The partial  $\beta$ -decay half-lives of  $^{188}\text{Bi}$ , considering both the  $\beta^+$  and electron-capture (EC) decay modes, were estimated within the fully self-consistent proton-neutron QRPA method using the same finite-range DIM Gogny interaction [18]. Although the HFB calculations are performed within the equal filling approximation, the present QRPA calculation breaks the time-reversal symmetry allowing to treat low- and high-spin states differently. This implies that Gamow-Teller  $\beta$ -strength functions are spin dependent and differ for ground and excited states. Axially symmetric deformations were consistently taken into account, both in the description of the decaying states and spin-isospin excitations. To empirically include the contribution beyond the 1-particle–1-hole excitations and the interaction between the single-particle and low-lying collective phonon degrees of freedom, a renormalization procedure, similar to the one found for the  $M1$  QRPA strength [18,36] was applied to the Gamow-Teller strength. The DIM+QRPA  $\beta$ -decay half-lives reproduce experimental data for neutron-deficient nuclei with a root-mean-square (rms) deviation of 5.9 on the ratio of theoretical to experimental values for the 505 nuclei with experimental half-lives lower than 1000 s lying between iron and polonium, and only 3.3 for the 49 nuclei lying between platinum and polonium.

Theoretically, the  $\beta\text{DF}$  probabilities (both for the  $\beta^+$  and EC modes) have been estimated on the basis of a detailed Hauser-Feshbach calculation of the competition between the fission and electromagnetic de-excitation channels. The excited states in the daughter nucleus  $^{188}\text{Pb}$  are assumed to be populated by the Gamow-Teller transitions to spins  $I_f = I_i \pm 1$ , where  $I_i$  is the spin in the mother nucleus and  $I_f$  is the spin in the daughter nucleus with the same parity. The

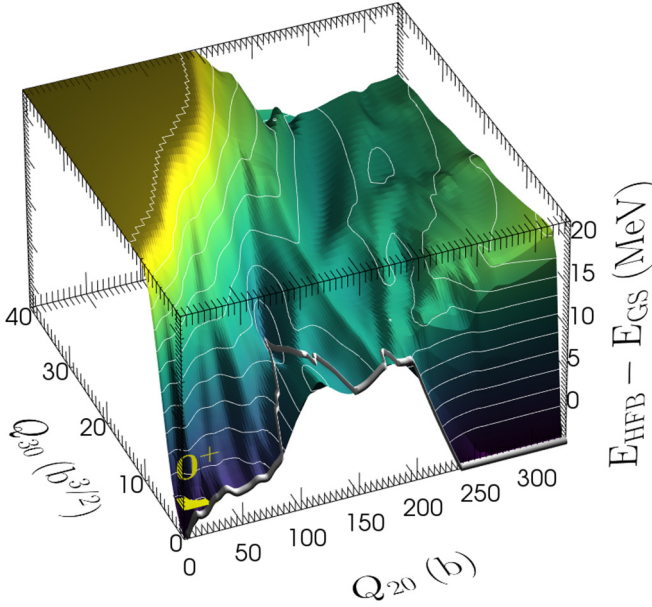


FIG. 10. Two-dimensional PES of  $^{188}\text{Pb}$  as a function of the axial quadrupole  $Q_{20}$  and octupole  $Q_{30}$  moments obtained with DIM interaction. The static fission path is shown by the thick gray line. The energy  $E_{\text{GS}}$  corresponds to the  $0^+$  ground state (marked by yellow surface with  $0^+$  label) at 3.4 MeV above the mean-field minimum.

$\beta$ DF probabilities are estimated by the TALYS code [37] with microscopic nuclear ingredients, in particular, nuclear level densities derived from the HFB plus combinatorial approach with the same DIM interaction [38] and the  $E1$  and  $M1$  strength functions obtained within the DIM+QRPA+Olim model [39]. The fission path (including the effective inertia) is estimated within the same Gogny-HFB mean-field calculation, as described in Ref. [40].

The DIM two-dimensional PES of  $^{188}\text{Pb}$  is shown in Fig. 10 as a function of the axial quadrupole  $Q_{20}$  and octupole  $Q_{30}$  moments. The height of the barrier ( $B_f$ ) amounts to about 11.0 MeV with respect to the  $0^+$  ground state shown in Fig. 10, which is higher than  $Q_{\text{EC}}(^{188}\text{Bi}) = 10.6$  MeV [28], leading to  $Q_{\text{EC}} - B_f < 0$ . This negative value would only allow for the subbarrier  $\beta$  feeding, resulting in a longer theoretical  $\beta$ DF half-life than experimentally observed. Thus, a global reduction of the fission path has been applied in order to reproduce  $T_{1/2p,\beta\text{DF}}(^{188}\text{Bi}^{\text{hs}}) = 5.6(8) \times 10^3$  s. The reduction factor amounts to 0.72, decreasing the primary fission barrier to a value of about 7.9 MeV and thus allowing a degree of above-barrier feeding. A similar decrease of the theoretical fission barriers was found to be needed in order to reproduce cross sections of complete-fusion reactions leading to polonium and bismuth compound nuclei [41]. The case closest to  $^{188}\text{Pb}$  was the compound nucleus  $^{188}\text{Bi}$ , for which a reduction factor of  $\approx 0.65$  had to be applied on the liquid-drop part of the fission barrier in the statistical-model code HIVAP. Moreover, a decrease of the  $^{178,180}\text{Hg}$  theoretical fission barriers by  $\approx 10$ –40%, depending on multiple parameters, was suggested in Ref. [42] to explain  $P_{\beta\text{DF}}$  values measured for  $^{178,180}\text{Tl}$ .

TABLE III. Theoretical spectroscopic properties, partial  $\beta$ -decay ( $T_{1/2p,\beta}$ ) and  $\beta$ DF ( $T_{1/2p,\beta\text{DF}}$ ) half-lives as well as the resulting  $\beta$ DF probabilities [ $P_{\beta\text{DF}}$ , see Eq. (3)] of  $^{188}\text{Bi}^{\text{hs}}$  [ $I^\pi = (10^-)$ ] and of the five lowest-lying prolate  $I^\pi = 1^+$  states with positive magnetic moments.  $K_\pi$  ( $K_v$ ) corresponds to the projection of the proton (neutron) spin and parity of the state. The excitation energy of the  $10^-$  state used in calculations was estimated to be  $\approx 150$  keV; see text for details.

$\beta_{20}$	$K_\pi$	$K_v$	$I^\pi$	$T_{1/2p,\beta}$ (s)	$T_{1/2p,\beta\text{DF}}$ (s)	$P_{\beta\text{DF}}$
-0.07	$9/2^-$	$11/2^+$	$10^-$	25.7	$5.5 \times 10^3$	$4.7 \times 10^{-3}$
0.35	$1/2^+$	$1/2^+$	$1^+$	0.8	$1.6 \times 10^3$	$5.1 \times 10^{-4}$
0.30	$1/2^-$	$1/2^-$	$1^+$	2.6	$2.2 \times 10^3$	$1.2 \times 10^{-3}$
0.26	$3/2^-$	$1/2^-$	$1^+$	3.0	$2.4 \times 10^3$	$1.3 \times 10^{-3}$
0.27	$1/2^-$	$1/2^-$	$1^+$	4.6	$3.2 \times 10^3$	$1.4 \times 10^{-3}$
0.33	$1/2^+$	$1/2^+$	$1^+$	1.9	$1.6 \times 10^3$	$1.2 \times 10^{-3}$

After reduction of the theoretical fission barrier, low-spin states which could correspond to  $^{188}\text{Bi}^{\text{ls}}$  were investigated. Based on laser-spectroscopy studies [13], the most likely shape, and spin and parity assignment of  $^{188}\text{Bi}^{\text{ls}}$  is a prolate  $I^\pi = (1^+)$  with a positive magnetic moment. Additionally, it can be tentatively determined based on the decay scheme proposed in the  $\alpha$ -decay spectroscopy study of  $^{192}\text{At} \rightarrow ^{188}\text{Bi}$  [43], that  $^{188}\text{Bi}^{\text{ls}}$  is the ground state and  $^{188}\text{Bi}^{\text{hs}}$  lies  $\approx 150$  keV above. Therefore, the  $\beta$ -decay properties of the various prolate  $I^\pi = 1^+$  states have been theoretically studied and are given in Table III for the five of them with the lowest calculated energies and positive magnetic moments.

Note that, with respect to the  $\beta^+$  decay, the EC channel gives rise to larger delayed fission probabilities up to a factor of about 2 due to the larger  $Q$  value. However, the  $\beta^+$  decay is about 7 to 11 times faster than EC, so that the total  $\beta$ DF rate is dominated by the  $\beta^+$  component. The ratio of the total  $\beta^+$  and EC rates and delayed fission rates can be used to define an equivalent  $\beta$ DF probability as

$$P_{\beta\text{DF}} = \frac{\lambda_{\beta\text{DF}}}{\lambda_\beta} = \frac{\lambda_{\beta^+\text{DF}} + \lambda_{\text{ECDF}}}{\lambda_{\beta^+} + \lambda_{\text{EC}}}. \quad (3)$$

The resulting  $\beta$ DF probabilities are given in Table III.

The  $I^\pi = 1^+$  states with  $\beta_{20} = 0.35, 0.30, 0.26,$  and  $0.33$  have  $\beta$ DF partial half-lives consistent with the measured value of  $1.7(6) \times 10^3$  s for  $^{188}\text{Bi}^{\text{ls}}$ . Despite the fact that there are these four candidates for the  $^{188}\text{Bi}^{\text{ls}}$  configuration, there is a clear trend of lower theoretical  $P_{\beta\text{DF}}$  values: All of these candidates have a  $P_{\beta\text{DF}}$  a factor of 4–9 lower than  $^{188}\text{Bi}^{\text{hs}}$ , thus hinting at a lower fission probability for low-spin states.

### B. FFMD calculations

As mentioned in Sec. I,  $^{188}\text{Pb}$  lies in the transitional region between nuclei with symmetric and asymmetric FFMDs, which makes the theoretical description of FFMD challenging. The fully microscopic scission-point model, known as SPY [44], predicts a symmetric FFMD for  $^{188}\text{Pb}$  (Fig. 11) using the same DIM binding energies. The single free parameter, the proton density at scission neck, is adjusted to

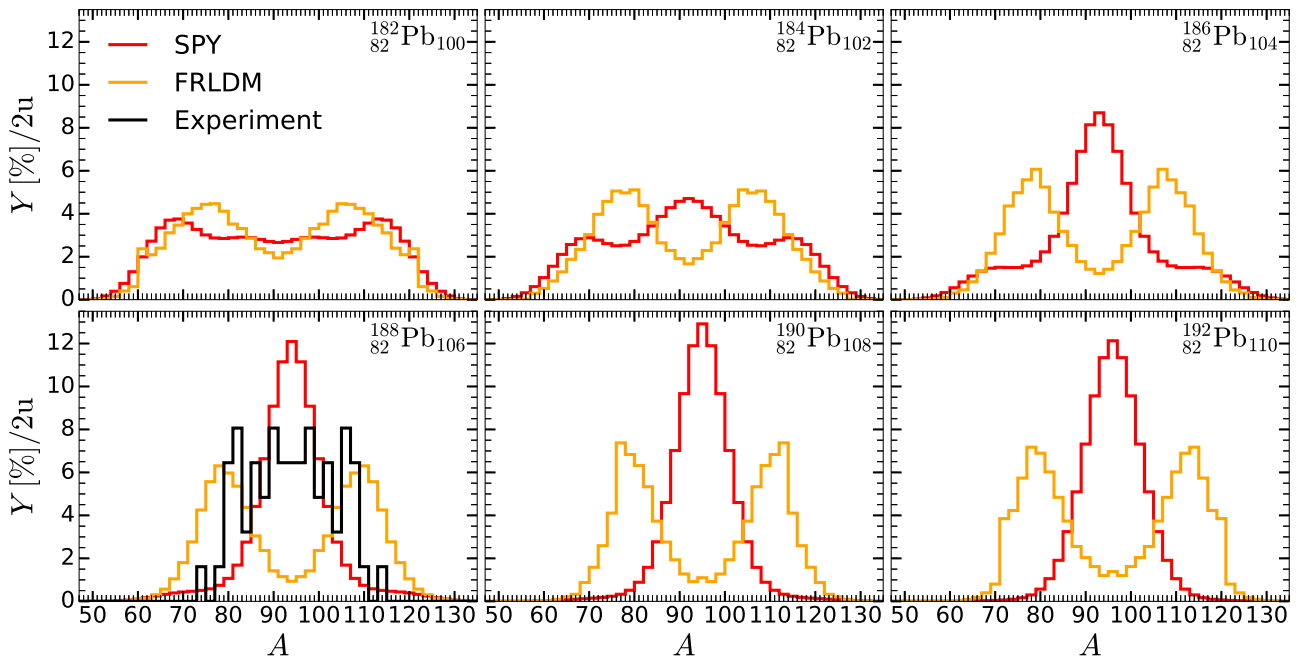


FIG. 11. Theoretical pre-neutron-emission FFMDs for the even-even isotopes  $^{182-192}\text{Pb}$ . The red (dark gray) line shows the results obtained with the SPY model [40] using the D1M-Gogny interaction. An excitation energy of 10 MeV is considered in all cases. The yellow (light gray) line represents the FRLDM-based calculations of Ref. [48] (these distributions are also available in supplemental online material for Ref. [49]). The present measurement for  $^{188}\text{Pb}$  is shown by the black histogram. All distributions, including the experimental one, are normalized to a total integral of 100%.

reproduce the experimental  $\overline{\text{TKE}} = 135.1(19)$  MeV. From an energy balance point of view, neither the  $N = 50$  nor the  $Z = 50$  shell closures play a significant role for the heavy fragments; i.e., they are not strong enough to be able to favor an asymmetric splitting. Similarly to  $^{180}\text{Hg}$ , it is not possible to explain the fission mode with arguments solely based on spherical shell closures [45]. Indeed, the Coulomb repulsion between the fragments also plays an important role, favoring fragments with prolate deformations, while shell closures tend to prefer spherical shapes. In addition, octupole deformation could also play a role as outlined in Refs. [46,47].

In contrast to SPY, the macroscopic-microscopic calculation based on the finite-range liquid-drop model (FRLDM) [48,49] predicts a fully asymmetric FFMD for  $^{188}\text{Pb}$  (Fig. 11). Therefore, neither of the models reproduces the experimental mixed-mode FFMD. To investigate this discrepancy, we consider neighboring even-even isotopes (Fig. 11). Both the FRLDM and SPY models predict predominantly asymmetric FFMD for  $^{182}\text{Pb}$ . When moving toward heavier isotopes up to  $^{192}\text{Pb}$ , FRLDM shows a transition to fully asymmetric FFMDs, while SPY predicts the opposite, a transition to fully symmetric FFMDs, thus again stressing the complexity of the precise determination of the border between symmetric and asymmetric mass splits.

For completeness, we mention the very recent results obtained using PES based on Lublin-Strasbourg drop (LSD) macroscopic energy and Yukawa-folded single-particle potential, where an extended region between platinum and radium was calculated [50]. This approach suggests a coexistence of two fission modes for the even-even isotopes  $^{182-192}\text{Pb}$  (Fig. 6 in Ref. [50]).

## VI. CONCLUSIONS

The  $\beta$ -delayed fission ( $\beta\text{DF}$ ) from low- and high-spin isomers in  $^{188}\text{Bi}$  was studied. By employing isomer-selective laser ionization and time gating, using the difference in half-lives of the states, we established that both isomers decay via  $\beta\text{DF}$ . The  $\beta\text{DF}$  partial half-lives and probabilities were determined for each isomer separately. For  $^{188}\text{Bi}^{\text{hs}}$ , we deduced a fission fragment mass distribution which could be explained by a mixture of symmetric and asymmetric modes. A mean total kinetic energy of 135.1(19) MeV for the  $\beta\text{DF}$  of  $^{188}\text{Bi}^{\text{hs}}$  was evaluated.

The first identification of  $\beta\text{DF}$  for  $^{190}\text{Bi}$  was made via the observation of a single fission event. Estimates of  $T_{1/2p,\beta\text{DF}}$  for the two long-lived states in  $^{190}\text{Bi}$  were evaluated. The results for  $^{190}\text{Bi}$  and  $^{188}\text{Bi}^{\text{hs,ls}}$  are consistent with the linear trend of  $\log_{10}(T_{1/2p,\beta\text{DF}})$  values (as a function of differences between  $Q_\beta$  values and fission barrier heights) in the neutron-deficient region.

The results for  $^{188}\text{Bi}$  were compared with self-consistent theoretical calculations based on a mean-field approach using the finite-range Gogny D1M interaction. The theoretical fission barrier of  $^{188}\text{Pb}$  was scaled down by  $\approx 30\%$  in order to reproduce the  $T_{1/2p,\beta\text{DF}}$  value measured for  $^{188}\text{Bi}^{\text{hs}}$ . After this reduction, a consistency of the measured  $T_{1/2p,\beta\text{DF}}(^{188}\text{Bi}^{\text{ls}})$  with a number of possible configurations for the prolate-deformed  $I^\pi = 1^+$  state was observed. Theoretical  $P_{\beta\text{DF}}$  values for these configurations were a factor of 4–9 lower than for  $^{188}\text{Bi}^{\text{hs}}$ . We compared the experimental fission fragment mass distribution from  $\beta\text{DF}$  of  $^{188}\text{Bi}^{\text{hs}}$  to our calculation of the distribution based on the scission-point model SPY and

to calculations based on the finite-range liquid-drop model. The mass distributions from both theoretical approaches differ and are in disagreement with the experimental results, which demonstrates the intricacy of the precise localization of the transition between symmetric and asymmetric fission modes.

### ACKNOWLEDGMENTS

We thank P. Moller for sharing data files for fission fragment mass distributions based on FRLDM, the ISOLDE Collaboration for providing excellent beams, and the GSI Target Group for manufacturing the carbon foils. This work

has been supported by the Fonds de la Recherche Scientifique (FNRS, Belgium) and the Research Foundation Flanders (FWO, Belgium) under the EOS Project No. O022818F, by GOA/2015/010 (BOF KU Leuven), the Interuniversity Attraction Poles Programme initiated by the Belgian Science Policy Office (BriX network P7/12), by the European Union's Horizon 2020 research and innovation programme under Grant Agreement No. 654002 (ENSAR2), by the U.K. Science and Technology Facilities Council, by the Slovak Research and Development Agency (Contracts No. APVV-14-0524 and No. APVV-18-0268), by the Slovak grant agency VEGA (Contract No. 1/0532/17), and by RFBR according to Research Project No. 19-02-00005.

- 
- [1] A. N. Andreyev, K. Nishio, and K.-H. Schmidt, *Rep. Prog. Phys.* **81**, 016301 (2018).
- [2] A. N. Andreyev, M. Huyse, and P. Van Duppen, *Rev. Mod. Phys.* **85**, 1541 (2013).
- [3] A. N. Andreyev, J. Elseviers, M. Huyse, P. Van Duppen, S. Antalic, A. Barzakh, N. Bree, T. E. Cocolios, V. F. Comas, J. Diriken *et al.*, *Phys. Rev. Lett.* **105**, 252502 (2010).
- [4] J. Elseviers, A. N. Andreyev, M. Huyse, P. Van Duppen, S. Antalic, A. Barzakh, N. Bree, T. E. Cocolios, V. F. Comas, J. Diriken *et al.*, *Phys. Rev. C* **88**, 044321 (2013); **102**, 019908(E) (2020).
- [5] A. N. Andreyev, S. Antalic, D. Ackermann, L. Bianco, S. Franchoo, S. Heinz, F. P. Heßberger, S. Hofmann, M. Huyse, Z. Kalaninová *et al.*, *Phys. Rev. C* **87**, 014317 (2013).
- [6] J. F. W. Lane, A. N. Andreyev, S. Antalic, D. Ackermann, J. Gerl, F. P. Heßberger, S. Hofmann, M. Huyse, H. Kettunen, A. Kleinböhl *et al.*, *Phys. Rev. C* **87**, 014318 (2013).
- [7] L. Ghys, A. N. Andreyev, M. Huyse, P. Van Duppen, S. Sels, B. Andel, S. Antalic, A. Barzakh, L. Capponi, T. E. Cocolios *et al.*, *Phys. Rev. C* **90**, 041301(R) (2014).
- [8] Y. A. Lazarev, Yu. Ts Oganessian, I. V. Shirokovsky, S. P. Tretyakova, V. K. Utyonkov, and G. V. Buklanov, *Europhys. Lett.* **4**, 893 (1987).
- [9] Y. A. Lazarev, Yu. Ts Oganessian, I. V. Shirokovsky, S. P. Tretyakova, V. K. Utyonkov, and G. V. Buklanov, *Inst. Phys. Conf. Ser.* **132**, 739 (1993).
- [10] A. N. Andreyev, D. Ackermann, S. Antalic, H. J. Boardman, P. Cagarda, J. Gerl, F. P. Heßberger, S. Hofmann, M. Huyse, D. Karlgren *et al.*, *Eur. Phys. J. A* **18**, 39 (2003).
- [11] M. J. G. Borge and B. Jonson, *J. Phys. G: Nucl. Part. Phys.* **44**, 044011 (2017).
- [12] R. Catherall, W. Andreatza, M. Breitenfeldt, A. Dorsival, G. J. Focker, T. P. Gharsa, T. J. Giles, J.-L. Grenard, F. Locci, P. Martins *et al.*, *J. Phys. G: Nucl. Part. Phys.* **44**, 094002 (2017).
- [13] C. Raison *et al.* (unpublished).
- [14] K.-H. Schmidt, S. Steinhäuser, C. Böckstiegel, A. Grewe, A. Heinz, A. R. Junghans, J. Benlliure, H.-G. Clerc, M. de Jong, J. Müller *et al.*, *Nucl. Phys. A* **665**, 221 (2000).
- [15] J. D. McDonnell, W. Nazarewicz, J. A. Sheikh, A. Staszczak, and M. Warda, *Phys. Rev. C* **90**, 021302(R) (2014).
- [16] T. Ichikawa, A. Iwamoto, P. Möller, and A. J. Sierk, *Phys. Rev. C* **86**, 024610 (2012).
- [17] S. Goriely, S. Hilaire, M. Girod, and S. Péru, *Phys. Rev. Lett.* **102**, 242501 (2009).
- [18] M. Martini, S. Péru, and S. Goriely, *Phys. Rev. C* **89**, 044306 (2014).
- [19] V. Fedosseev, K. Chrysalidis, T. Day Goodacre, B. Marsh, S. Rothe, C. Seiffert, and K. Wendt, *J. Phys. G: Nucl. Part. Phys.* **44**, 084006 (2017).
- [20] V. N. Fedoseyev, G. Huber, U. Köster, J. Lettry, V. I. Mishin, H. Ravn, and V. Sebastian, *Hyperfine Interact.* **127**, 409 (2000).
- [21] S. Rothe, T. Day Goodacre, D. V. Fedorov, V. N. Fedosseev, B. A. Marsh, P. L. Molkanov, R. E. Rossel, M. D. Seliverstov, M. Veinhard, and K. D. A. Wendt, *Nucl. Instrum. Methods B* **376**, 91 (2016).
- [22] B. Lommel, W. Hartmann, B. Kindler, J. Klemm, and J. Steiner, *Nucl. Instrum. Methods A* **480**, 199 (2002).
- [23] M. D. Seliverstov, T. E. Cocolios, W. Dexters, A. N. Andreyev, S. Antalic, A. E. Barzakh, B. Bastin, J. Büscher, I. G. Darby, D. V. Fedorov, *Phys. Rev. C* **89**, 034323 (2014).
- [24] A. Rytz, *At. Data Nucl. Data Tables* **47**, 205 (1991).
- [25] L. Ghys, Ph.D. thesis, KU Leuven, Belgium, 2015 (unpublished).
- [26] J. Wauters, P. Dendooven, M. Huyse, G. Reusen, P. Van Duppen, R. Kirchner, O. Klepper, and E. Roeckl, *Z. Phys. A* **345**, 21 (1993).
- [27] A. N. Andreyev, N. Bijnens, M. Huyse, P. Van Duppen, M. Leino, T. Enqvist, P. Kuusiniemi, W. Trzaska, J. Uusitalo, N. Fotiades *et al.*, *J. Phys. G: Nucl. Part. Phys.* **25**, 835 (1999).
- [28] M. Wang, G. Audi, F. G. Kondev, W. J. Huang, S. Naimi, and Xing Xu, *Chin. Phys. C* **41**, 030003 (2017).
- [29] W. D. Myers and W. J. Świątecki, *Phys. Rev. C* **60**, 014606 (1999).
- [30] P. Möller, J. R. Nix, W. D. Myers, and W. J. Świątecki, *At. Data Nucl. Data Tables* **59**, 185 (1995).
- [31] L. Ghys, A. N. Andreyev, S. Antalic, M. Huyse, and P. Van Duppen, *Phys. Rev. C* **91**, 044314 (2015).
- [32] G. L. Wilson, M. Takeyama, A. N. Andreyev, B. Andel, S. Antalic, W. N. Catford, L. Ghys, H. Haba, F. P. Heßberger, M. Huang *et al.*, *Phys. Rev. C* **96**, 044315 (2017).
- [33] J. Konki, J. Khuyagbaatar, J. Uusitalo, P. T. Greenlees, K. Auranen, H. Badran, M. Block, R. Briselet, D. M. Cox, M. Dasgupta *et al.*, *Phys. Lett. B* **764**, 265 (2017).

- [34] A. N. Andreyev, D. D. Bogdanov, S. Saro, G. M. Ter-Akopian, M. Veselsky, and A. V. Yeremin, *Phys. Lett. B* **312**, 49 (1993).
- [35] V. L. Truesdale, A. N. Andreyev, L. Ghys, M. Huyse, P. Van Duppen, S. Sels, B. Andel, S. Antalic, A. Barzakh, L. Capponi *et al.*, *Phys. Rev. C* **94**, 034308 (2016).
- [36] S. Goriely, S. Hilaire, S. Péru, M. Martini, I. Deloncle, and F. Lechaftois, *Phys. Rev. C* **94**, 044306 (2016).
- [37] A. J. Koning and D. Rochman, *Nucl. Data Sheets* **113**, 2841 (2012).
- [38] S. Hilaire, M. Girod, S. Goriely, and A. J. Koning, *Phys. Rev. C* **86**, 064317 (2012).
- [39] S. Goriely, S. Hilaire, S. Péru, and K. Sieja, *Phys. Rev. C* **98**, 014327 (2018).
- [40] J.-F. Lemaître, S. Goriely, S. Hilaire, and N. Dubray, *Phys. Rev. C* **98**, 024623 (2018).
- [41] A. N. Andreyev, D. Ackermann, S. Antalic, I. G. Darby, S. Franchoo, F. P. Heßberger, S. Hofmann, M. Huysec, P. Kuusiniemi, B. Lommel *et al.*, *Phys. Rev. C* **72**, 014612 (2005).
- [42] M. Veselský, A. N. Andreyev, S. Antalic, M. Huyse, P. Möller, K. Nishio, A. J. Sierk, P. Van Duppen, and M. Venhart, *Phys. Rev. C* **86**, 024308 (2012).
- [43] A. N. Andreyev, S. Antalic, D. Ackermann, S. Franchoo, F. P. Heßberger, S. Hofmann, M. Huyse, I. Kojouharov, B. Kindler, P. Kuusiniemi *et al.*, *Phys. Rev. C* **73**, 024317 (2006).
- [44] J.-F. Lemaître, S. Goriely, S. Hilaire, and J.-L. Sida, *Phys. Rev. C* **99**, 034612 (2019).
- [45] S. Panebianco, J.-L. Sida, H. Goutte, J. F. Lemaître, N. Dubray, and S. Hilaire, *Phys. Rev. C* **86**, 064601 (2012).
- [46] G. Scamps and C. Simenel, *Phys. Rev. C* **100**, 041602(R) (2019).
- [47] G. Scamps and C. Simenel, *Nature (London)* **564**, 382 (2018).
- [48] P. Möller (private communication).
- [49] P. Möller and J. Randrup, *Phys. Rev. C* **91**, 044316 (2015).
- [50] K. Pomorski, A. Dobrowolski, R. Han, B. Nerlo-Pomorska, M. Warda, Z. Xiao, Y. Chen, L. Liu, and J.-L. Tian, *Phys. Rev. C* **101**, 064602 (2020).